Carson, B., Westbrook, G.K., Musgrave, R.J., and Suess, E. (Eds.), 1995
Proceedings of the Ocean Drilling Program, Scientific Results, Vol. 146 (Pt. 1)

12. MICROSTRUCTURES IN ACCRETED SEDIMENTS OF THE CASCADIA MARGIN[1]

Ben Clennell[2] and Alex Maltman[3]

ABSTRACT

Deformed sediments collected from drilling at the Cascadia forearc were examined using optical and electron microscopy. A wide range of microstructures was encountered in a sample suite consisting mainly of fine-grained sediments. Most of the samples were recovered from the Oregon sector of the accretionary wedge, at Site 891, located at the deformation front, and Site 892, located on the second thrust ridge. For purposes of comparison, we also examined a small number of samples from the undeformed Cascadia Basin (Site 888) and from behind the second thrust ridge at the Vancouver Margin (Sites 889 and 890).

Within each site, there is a strong compositional control on the style of deformation. Diatomaceous silts tend to show a more brittle style of deformation than either clay-rich silts or sands. Arrays of subparallel shear zones and incipiently scaly textures are developed in clay-rich sediments.

At Site 891, intense deformation is largely confined to the vicinity of fault zones, where thick (tens of meters) intervals of incipiently scaly fabric and thin (tens of centimeters) zones of fault gouge are developed. Chaotic, small-scale folding is present at several horizons, and, in some cases, is overprinted by shear zones.

Deformation at Site 892 is much more pervasive, with widespread fracturing producing a mosaic-like microstructure of angular blocky fragments. We interpret the blocky fractured texture as evidence for previous high pore fluid pressures and natural hydraulic fracturing within the Cascadia accretionary prism. Intervals of intense fracturing are transitional into a "pillow-in-matrix" structure consisting of subrounded blocks of intact sediment within a sheared, clay-rich matrix. Darkened zones of gouge and broken formation, several meters thick, are interpreted as the main fault zones that have previously conducted fluids from depth, so that the fault rocks were chemically altered and mineralized.

INTRODUCTION

Study Objectives

Two of the principal scientific objectives of Ocean Drilling Program Leg 146 were to investigate the relative roles of diffuse and focused flow in controlling the fluid budgets of accretionary prisms, and to gather information on how fluid flow and deformation may be coupled in these systems (e.g., Karig, 1990; Westbrook, 1991; MacKay et al., 1992; Moore and Vrolijk, 1992). To this end, we examined sediments sampled from deformed parts of the wedge and attempted to relate their microstructural and diagenetic features to their stress, strain, and fluid-flow history.

Tectonic and Sedimentological Setting

The Cascadia Margin is a site of active accretion, where a heterogeneous sequence of Neogene to Holocene sediments is scraped off the Juan de Fuca Plate as it subducts beneath the northwestern margin of North America (Cochrane et al., 1994; Hyndman et al., 1994; Shipboard Scientific Party, 1994) (Fig. 1). The predominant sediments are silty clays, diatomaceous clayey silts and sands (Westbrook, Carson, Musgrave, et al., 1994).

Site 888 lies 7 km seaward of the deformation front, offshore from Vancouver Island, and penetrates undeformed, sandy sediments deposited at the fringe of the Pleistocene to Holocene Nitinat Fan. Sites 889 and 890 are also located in the Vancouver segment of the Cascadia accretionary prism, 9 km landward of the deformation front. Drilling there penetrated Pleistocene to Holocene slope basin sediments and then entered older accreted material.

Two sites were located in the Oregon segment of the Cascadia prism. Drilling at Site 891 penetrated the younger, sand-rich sequence at the frontal thrust, while Site 892 was situated on the second ridge. Five holes drilled at Site 892 encountered deformed, accreted material after penetrating a thin veneer of recent slope sediments. The accreted sediments at Site 892 were again found to be predominantly fine-grained, with clayey silts similar to those at Sites 889 and 890 ranging in age from late Miocene to late Pliocene.

Sampling Strategy

Poor overall core recovery precluded collecting material on a very systematic basis. All the samples examined were collected away from drilling disturbance. Oriented samples of 20–60 cm^3 volume were cut from the center of the split core with a sharp knife and immediately sealed in plastic containers to prevent drying. The final sample suite we describe consists of silty clays, clayey silts, and sands from both fault zone and "undeformed" environments within the seaward (Site 891) and internal (Sites 889, 890, and 892) parts of the wedge. Material was also collected from the undeformed reference site (Site 888). The latter material was not studied in detail, but enabled us to conclude that our careful sampling and preparation methods did not introduce artifacts that we could misinterpret as tectonic features.

METHODS

Standard thin sections were made of air-dried, resin-impregnated samples and were examined using conventional light microscopy. Broken surfaces of air-dried samples were examined using an Hitachi S2400 scanning electron microscope (SEM) in secondary electron

[1]Carson, B., Westbrook, G.K., Musgrave, R.J., and Suess, E. (Eds.), 1995. *Proc. ODP, Sci. Results,* 146 (Pt. 1): College Station, TX (Ocean Drilling Program).

[2]Department of Earth Sciences, University of Leeds, Leeds LS2 9JT, England, United Kingdom.

[3]Institute of Earth Studies, University of Wales, Aberystwyth, Dyfed SY23 3DB, Wales, United Kingdom.

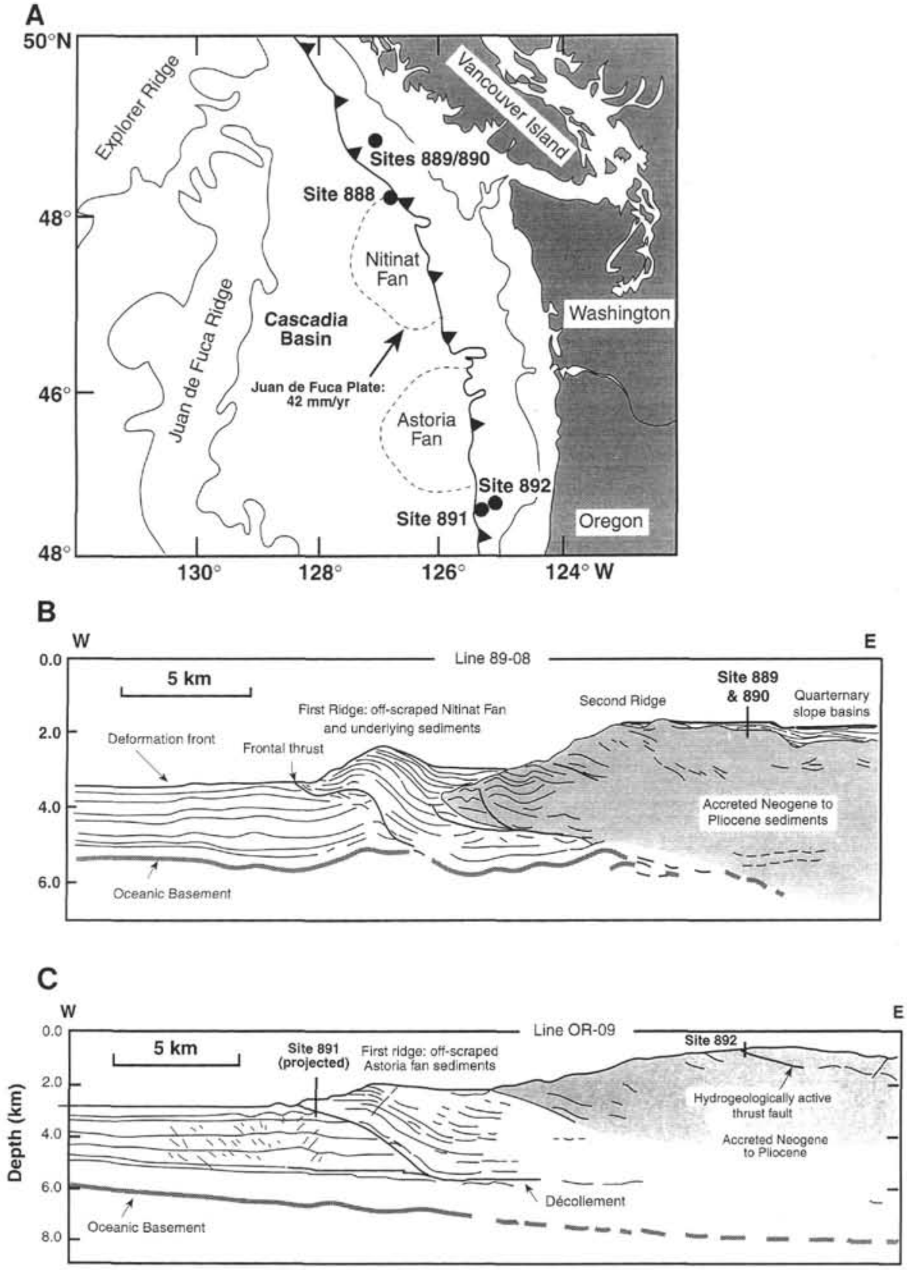

Figure 1. Location of Leg 146 drill sites. **A.** Key map showing section lines based on multichannel seismic data. **B.** Interpretative drawing of line 89–08 off Vancouver Island showing the position of Sites 889 and 890 on a plateau region behind the second thrust ridge. **C.** Interpretative drawing of line OR-09 showing location of Site 892 on the second thrust ridge. The location of Site 891 is projected along strike from about 3 km to the south. After Westbrook (1994).

mode. Polished thin sections and resin-impregnated blocks were imaged using a Jeol 5300 and Camscan Series 200 SEM operating in backscattered electron (BSE) mode, which is sensitive to mineral composition and density though mean atomic number contrast. In this way, the fabrics were observed from centimetric down to submicron scales. A small number of samples were examined while still wet using a Jeol low-vacuum scanning electron microscope that does not require any coating or other preparation of the samples. The low-vacuum instrument uses a modified BSE detector that is largely sensitive to secondary electrons but gives some compositional signal. While the resolution of this instrument is less than the standard SEM, we were able to confirm that no important artifacts were introduced during slow air drying of the samples.

OBSERVATIONS

Site 888

The silty clays from Site 888 show a moderate to high degree of preferred particle orientation (e.g., Sample 146-888B-7H6, 40–42 cm, from 60.92 meters below seafloor), although presumably they have undergone no strain other than burial consolidation. None of the samples examined show any tectonic deformation features. Where seen, bedding is subhorizontal, and magnetic fabrics from this site show oblate strain ellipsoids typical of burial consolidation (Westbrook, Carson, Musgrave, et al., 1994). This confirms the inference from the seismic survey that deformation as a precursor to accretion does not propagate more than 2 to 3 km from the wedge toe in this region. The sequence is normally consolidated throughout the cored interval (Westbrook, Carson, Musgrave, et al., 1994), indicating that although deformation extends ahead of the first thrust (Fig. 1), there is no proto-décollement zone similar, for example, to that found several kilometers ahead of the wedge toe at the Barbados Ridge (Moore, Mascle et al., 1990).

Sites 889 and 890

Sediments from the slope basin sequence (0–120 mbsf) are practically undeformed, apart from occasional gas expansion cracks. Low-vacuum and conventional electron microscope observations show that the initial sediment microfabrics are open with high porosity and little original lamination (Pl. 1). It is also evident that a high proportion of the fine-grained material, though, in the "clay fraction" as defined by grain size, actually consists of angular rock and mineral fragments rather than platy clay minerals. This observation also applies to most of the other fine-grained sediments from Cascadia, and has important implications for deformation behavior.

The remainder of the samples are from the accreted Pliocene sediments. Closely spaced joints and fractures are widespread throughout the core. Thin sections of samples from the fractured intervals show shear zones with very small displacements (100 μm to 3 mm) marked by thin (20 μm across) zones of clays with a preferred orientation. Some of these discontinuities extend for more than a centimeter, while others are less persistent and form *en échelon* sets. Volcanic glass fragments are incipiently altered to clay minerals. Abundant diatoms show no evidence of dissolution, but they are commonly broken.

While a few small fault zones are visible in the core, the general lack of more pervasive microstructures at this site indicates that the material was accreted to the wedge and elevated to its present position as large, intact blocks (e.g., Moore, 1989). There is no microstructural evidence of focused fluid flow, such as mineral veining or chemical alteration. This, and the lack of chemical cementation or dissolution of unstable grains (volcanic glass and diatoms), suggests that the sediment was not subjected to large fluxes of exogenous fluids.

Site 891

Core recovery from Hole 891 was very poor. The top of the penetrated sequence contains abnormally overconsolidated sediments with some contorted bedding, and is considered to be a slump mass (Westbrook, Carson, Musgrave, et al., 1994). Below this is a sand-dominated sequence of turbidites, extending down to 230 mbsf, that has few recognizable deformation features. Only cohesive sediments, from below this level, were examined. Figure 2 shows a summary of the structural features at Site 891.

A sample from 244 mbsf shows a variety of deformation features within the area of a single thin section (Pl. 2). These include millimeter-sized load balls and microfaulting of sandy laminae in a pattern indicative of stratal extension. It is not clear if these are of syn-sedimentary origin, are related to slumping, or were formed during tectonic deformation of sediment that still retained a high water content (e.g., Maltman, 1994). Adjacent sediments are completely undeformed, which is a possible indication that the features are related to very localized dewatering.

A sample from 265 mbsf is the only material examined from a putative fault zone on the structural log (Fig. 2). The sediment is a heterogeneous breccia of poorly sorted sand and siltstone fragments dispersed in a clay-rich matrix (see Westbrook, Carson, Musgrave, et al., 1994, pp. 258–259, fig. 22). Some of the clayey siltstone clasts are deformed in a ductile way, while others, presumably more lithified, have brittle fractures. Some of the clasts in the breccia have kink folds and small shear zones defined by planar preferred orientation of clay grains.

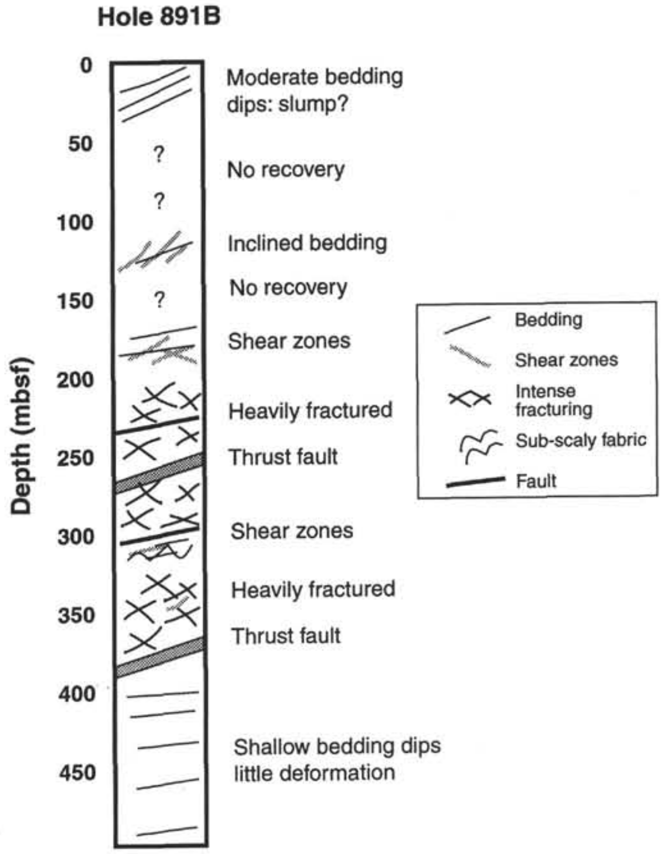

Figure 2. Graphic log of macroscopic structural features at Hole 891B, adapted from Westbrook, Carson, Musgrave, et al. (1994).

The next interval of Hole 891, down to about 360 mbsf, shows heterogeneous ductile deformation. Several samples are undeformed, or have inclined bedding that is not disrupted internally. Layers and patches of sand show no traces of cement, and the BSE images show no diagenetic minerals apart from abundant micro-framboidal pyrite (Pl. 3). The pore-size distribution in these sediments is very broad with larger pore spaces between aggregates of unsorted particles, and small intra-aggregate pores. There is no fabric of preferred orientation of the pore space, and some of the larger pores are bridged by trains of clays. Clay-rich layers show moderate particle preferred orientation but diatoms and thin mica flakes are unbroken and show no preferred orientation, indicating that compactional strain is not very intense in the these specimens.

By contrast, intervening samples from this interval show significant deformation. including small contorted folds, possible dewatering structures, mud injections, and diffuse zones of preferred planar orientation in clays. The sediments having this ductile deformational style are more poorly sorted than the intervening sediments that still display intact sedimentary structures: sand grains and sand patches appear to float in a clay and fine silt matrix, possibly as a result of clay infiltration. The sediment microfabric is not noticeably more compact than the nearby undeformed sediments, but all the diatoms found were broken, and fractures are common in the larger mica flakes.

A sample from 316 mbsf shows well-developed chevron folding in the sandy and silty layers giving a crenulated appearance (Fig. 3A). There is no accompanying brittle deformation, or any strong preferred orientation of clay grains. Backscattered electron imaging shows no obvious deformation, as the scale of the folds is larger than the 2 mm field of view of the instrument, and there are no associated microstructures. There is complete clay infiltration of all but the thickest sandy layers, and the general sediment microfabric appears compact, with few larger pores. Highly asymmetrical folds are developed in samples from 411 to 413 mbsf. There is a pervasive axial-planar orientation of clay and mica particles, but there are no accompanying brittle deformation features, such as narrow slip zones or fractures. These structures are interpreted as folds formed during initial shear that have been streaked out and dismembered by continued slip (Fig. 3B).

A sample from 349 mbsf has a range of ductile, syn-sedimentary deformation features. These include loadmarks and small diapir-like structures that are overprinted by thin shear zones. Some of the shear zones fan out and become dispersed in clay-rich portions of the sediment (Pl. 2). Although superficially similar to features described from 244 mbsf, the structures in this sample are more organized and compatible with surrounding tectonic deformation, and, thus, are not considered to be of syn-sedimentary origin.

Material from below about 330 mbsf, and particularly below 400 mbsf, is incipiently cemented by carbonate (Pl. 1). Two samples from 437 to 450 mbsf show localized brittle fractures that perhaps are related to slight cementation, along with thin shear zones and kink folds defined by clays with a common preferred orientation that are conspicuous under crossed polars. There is also compositional, rather than diagenetic, control on the deformation. Discrete shear zones (50–80 μm across) in clayey silt layers splay into numerous anastomosing zones of preferred particle orientation as they pass into more clay-rich parts of the sediment.

A sample examined from 447.81 mbsf shows ductile shear folds, similar to those at 411 mbsf and accompanied by later shear zones. Samples from below this depth show some inclined and slightly contorted bedding, but no fault zones or intense fracturing.

Summary of Site 891 Features

In general, the sediments from Site 891 show a heterogeneous style of deformation. Although recovery was very poor and sample disturbance was a problem, careful selection is believed to have reduced the number of artifacts recorded. There is a wide range of soft sediment deformation features, many of which, such as load marks and mini diapirs, can be ascribed to syn-sedimentary or early post-depositional settlement and dewatering. Other ductile features, such as sheared-out folds, are associated with a weak axial planar cleavage, and are tentatively interpreted to be of tectonic origin (but see Farrell and Eaton, 1988). The folds are sometimes overprinted in the same samples by more "brittle" (i.e., more localized) deformation features, such as thin shear zones and arrays of kink folds. The absence of microstructures typical of scaly clay (e.g., Cowan, 1985; Moore et al., 1986) is notable, even though some horizons have a high clay content and a macroscopic texture indicative of the incipient development of scaly fabric.

We interpret the interval from about 263 to about 265 mbsf as a breccia-filled fault zone. Material from the other fault zone indicated on the structural log of Site 891 at about 375 mbsf (Westbrook, Carson, Musgrave, et al., 1994) was not available for sampling.

We found no evidence for pervasive lithification, by compaction or cementation, of the sediments in the upper few hundred meters of the penetrated section, despite electric log indications of lithified horizons and the presence of scattered cemented nodules in the cores

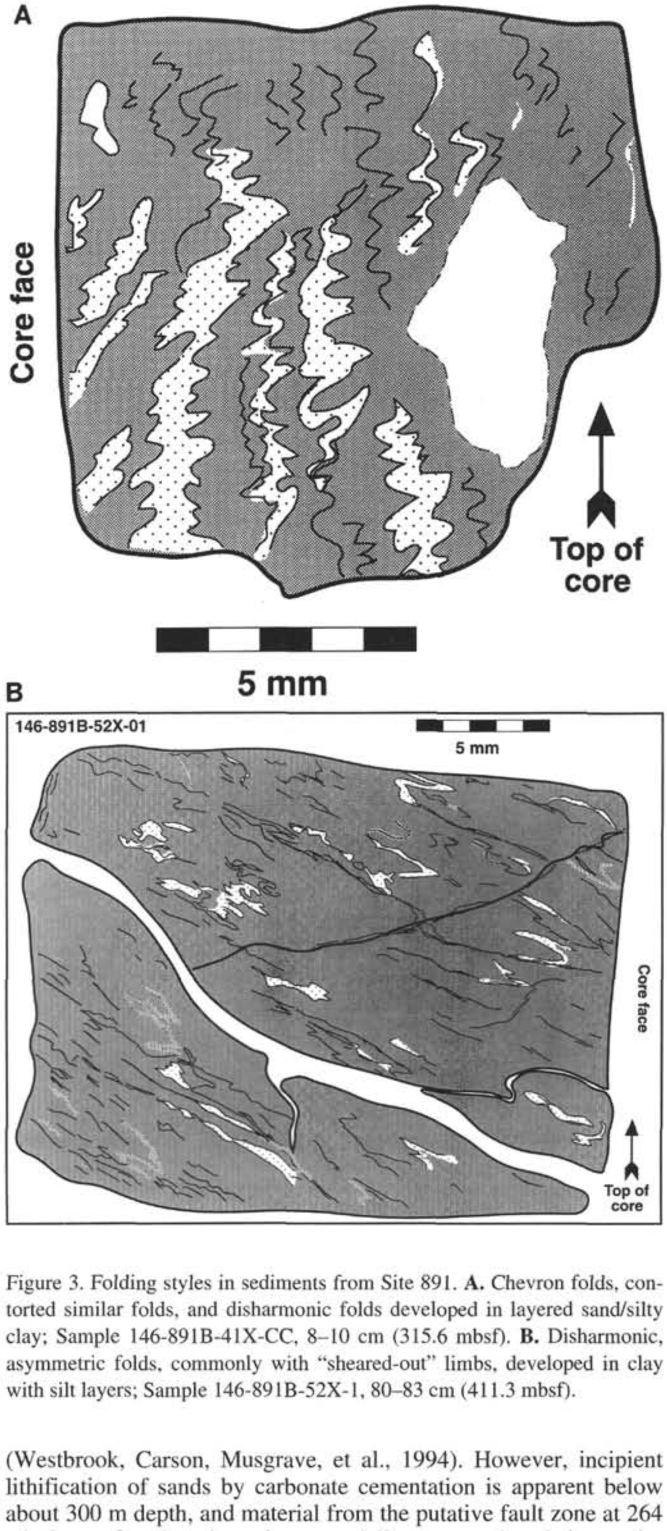

Figure 3. Folding styles in sediments from Site 891. **A.** Chevron folds, contorted similar folds, and disharmonic folds developed in layered sand/silty clay; Sample 146-891B-41X-CC, 8–10 cm (315.6 mbsf). **B.** Disharmonic, asymmetric folds, commonly with "sheared-out" limbs, developed in clay with silt layers; Sample 146-891B-52X-1, 80–83 cm (411.3 mbsf).

(Westbrook, Carson, Musgrave, et al., 1994). However, incipient lithification of sands by carbonate cementation is apparent below about 300 m depth, and material from the putative fault zone at 264 mbsf was found to have been partially cemented and then redeformed.

Site 892

The sediments from this site are lithologically homogenous, chiefly consisting of silts and clayey silts. Only one lithostratigraphic unit was identified from sedimentary logging of cores and smear-slide data. However, subsequent biostratigraphic studies showed that the sequence cored at Site 892 is made up of a number of intact sequences of different stratigraphic ages bound by discontinuities, interpreted as faults and unconformities. Only some of these boundaries can be matched with features visible on seismic sections, in the physical properties data, or in the structural logging of the core (Fig. 4). Several holes were drilled close together at the site, but even though they were cored and logged continuously, we could not link lithological and structural features between them with any confidence. The seismic lines show a series of discontinuous reflectors in this part of the wedge with only a few through-going features (Westbrook, Carson, Musgrave, et al., 1994). The latter are interpreted as the major faults. In contrast with Site 889, completely undeformed intervals of more than ~0.5 m are rare, and complex deformation features are present even at very shallow depths beneath the seafloor.

Surficial Sediments

Original sedimentary microstructures are recorded in two samples examined while still moist under low-vacuum SEM, from depths of 0.34 and 0.46 mbsf. Both samples are poorly sorted clay-bearing silts with many diatoms. They have an open structure of unoriented silt grains, unaltered volcanic glass fragments and siliceous skeletal debris, with a small clay mineral content (10%–30%). Most of the silt is less than 10 µm in diameter and much is in the "clay fraction" (<2 µm grain size). The relative lack of clay minerals accounts for the very low cohesion and brittle nature of the sediment after slight drying. The porosity is very heterogeneously distributed, with a few large pores adjacent to large grains and unbroken diatoms, and a fine network of inter-particle voids in the silt/clay matrix.

These two samples were subsequently dried at room temperature under vacuum, gold-coated, and re-examined under secondary electron imaging. The same fabrics are evident with no evidence of drying artifacts (Pl. 1). This probably reflects the silty nature of the sediments, and the fact that the clay mineralogy is dominated by illites and micas, rather than smectite minerals that are more sensitive to drying. The absence of artifacts is reassuring for the interpretation of other samples, which were dried slowly prior to resin impregnation and sectioning.

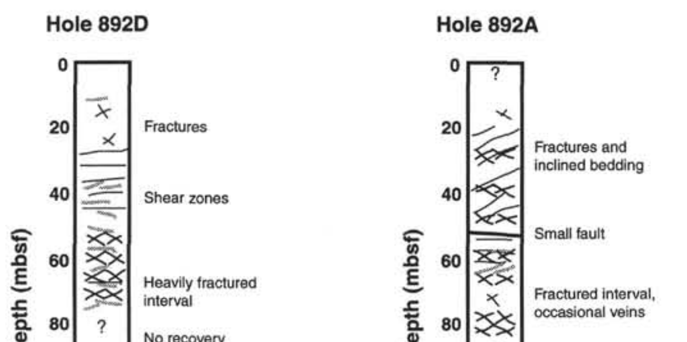

Figure 4. Graphic logs of macroscopic structural features at Site 892, adapted from Westbrook, Carson, Musgrave, et al. (1994).

Accreted Material

We have cataloged the samples in order of depth, rather than trying to fit the complex distribution of deformational features into any structurally based scheme. A more coherent zonation should emerge from integration of the post-cruise stratigraphic, structural, physical properties, and rock magnetic data.

Putative Fault Zone, 10 mbsf, Hole 892D

A sample from only 10.16 mbsf shows intensely developed sediment deformation features. Microscopically, the sediment is very heterogeneous, generally consisting of blocks of weakly to strongly cemented clayey silt, 100–1000 µm across in a sheared cataclastic matrix of altered clay and silt (Pl. 4). While most of the blocks are well-rounded, some are angular and fractured, with fine-grained, gouge-like material injected into the cracks. Clay-rich layers show ductile streaking and boudinage. The sediment is partly cemented by carbonate that also occurs as dispersed small crystals (ankerite). Broken fragments of ferroan dolomite show deformation twinning and crack-seal texture. There are some small (100 µm across) gypsum clusters, a number of which have been streaked out into the gouge. In places the gouge is slightly cemented by carbonate. There are no undeformed veins.

The clayey, brown-stained layers seen in the split core are brighter in back-scattered electron imaging due to greater compaction and have a higher content of iron, indicated by energy-dispersive x-ray analysis. We believe the brown clayey material is an alteration product of chemically unstable grains in the sediment (particularly volcanic glass and iron sulfides).

Shallow Fractured Interval, 30–80 mbsf

The macroscopic appearance of the sediment in this depth interval is jointed to incipiently scaly, with the firm sediment breaking up into many angular fragments (cf. Pl. 5, Figs. 1, 2). The fracture spacing is highly variable, so that the blocky fragments range in size from 0.5 mm to about 5 cm across. Intact blocks bounded by these fractures are compositionally very similar to the surficial sediments, mainly comprising diatomaceous silty clays and clayey silts. The sediments have a very much more compact fabric, with the clays squeezed between the silt grains to leave no large pores. Mica and volcanic glass grains are slightly altered to clays. These features indicate deformation at a deeper level of burial.

Typically, diatomaceous clayey silts in the fractured intervals develop a blocky "mosaic" structure comprising angular blocks divided by discrete fractures or shear zones 10 to 20 µm wide (Pl. 5, Fig. 2). Some of the fractures have offset the bedding lamination of adjacent blocks very slightly and other seams are apparently in an early stage of development, with no offset, or are discontinuous. There is a slight tendency for the fractures to intersect at angles of about 40 to 60 degrees, which could indicate that they formed as conjugate sets (e.g., Pl. 5, Fig. 2). However, the sense of displacement on fractures that do show some offset is not always consistent with an origin in a conjugate pair. Furthermore, the intersecting sets themselves are not consistently oriented in any one direction. The lack of a predominant orientation is also apparent from measurements of macroscopic structural features in the core (Westbrook, Carson, Musgrave, et al., 1994). The darker seams show no segregation of clays or opaque minerals, and so are difficult to discern in plane-polarized light. They are darker simply because they have a more compact fabric. Inside the shear zones, porosity is reduced due to breakage and collapse of the matrix of delicate diatom and radiolarian tests, and as a consequence of enhanced planar preferred orientation of clay minerals.

In many samples, this "mosaic structure" is transitional into closely spaced (50–200 µm apart) arrays of more diffuse shear zones that divide the sediment into rhombohedral blocks. The inter-block material is markedly darker than that of the blocks, and appears to have been partly altered to clay. In other samples, the general appearance is of subrounded, pillow-like blocks that float in a poorly sorted but generally fine-grained matrix. The "pillows" separated by the shear zones have different preferred particle orientations, that are occasionally swirled in nature (Pl. 5, Fig. 3). This suggests that not all the blocks were internally rigid, and the incipient ductile deformation has been cut through by thin shear zones. The sediments appear to have been partly cemented prior to lithification: patches of carbonate cemented silt "float" within the matrix of the shear zones. There are also small isolated patches of ferroan dolomite or ankerite, and stellate clusters of gypsum crystals, both of which appear to post-date the diffuse shear zones.

Samples from 38 and 47 mbsf are typical glauconitic silty clays from Site 892. Most of the glaucony is apparently redeposited, but some larger grains appear to have regrown over narrow shear zones that pervade the sediment (cf. Pl. 3, Fig. 4). Thin layers of carbonate silt and small patches of ferroan dolomite are undeformed and appear to have recrystallized after the shear zones were formed. The glaucony grains are commonly rimmed by a brownish high birefringence clay that is very similar in habit and optical properties to altered clays found concentrated in shear zones and inter-block areas.

Heterogeneous Deformation, 80–120 mbsf, Hole 892A

Samples from this interval show evidence of compositional control on the deformational style. A blocky mosaic texture is weakly developed in diatomaceous portions (diatoms ~40%, silt 40%, and clay 20%), while deformation is partitioned into the clay-rich portions lacking in diatoms (clay > 40%, diatoms < 20%), which have strongly developed shear zone arrays defining an incipiently scaly fabric. Brittle fractures defining the mosaic structure in diatomaceous clayey silts show much less preferred orientation than shear zones in the clay-rich sediments, which form closely spaced subparallel or anastomosing arrays.

Faulted Interval, 103–116 mbsf, Hole 892D

Samples of diatomaceous clayey silt from around 103 mbsf are pervaded by arrays of subparallel shear zones. While some of the zones are thin and similar to those defining the mosaic texture, most are much wider (50–100 µm across) and more diffuse at the edges. The shear zones are so dense and thick that they occupy about one third of the total area of the section. Viewed in the optical microscope, the zones appear slightly darker than the surrounding sediments and are only picked out by their phyllosilicate orientation visible in cross-polarized light. At high magnifications in BSE imaging, the shear zone interiors are seen to be more compact than the surrounding sediment and there is slightly more grain breakage within them. The grain breakage is apparently limited to weaker particles, such as diatoms, volcanic glass and mica.

The sediments in this interval are uncemented and unaltered, being similar in color to the overlying undeformed material. There is, however, the association noted earlier of yellowish-brown clay growing preferentially in the shear zones and also overgrowing a few isolated grains of glaucony. There are scattered patches of gypsum, growing as irregular clusters that have many included sediment particles and as more idiomorphic, twinned aggregates with trails of small fluid inclusions. The gypsum growth post-dates the shear zones, as some crystals are deformed. Gypsum crystals are found just as commonly in the undeformed areas as in the shear zones, so it is not suggested that the gypsum was necessarily precipitated from an exogenous fluid that had been carried along faults or fractures.

The sediments immediately below (104 to 115 mbsf) show pronounced macroscopic banding on a centimeter scale, and arrays of shear zones are evident in the core. The interval is considered to be a thick fault zone filled with gouge and micro-mélange (Westbrook, Carson, Musgrave, et al., 1994). The material has a dark brown color that is different from the surrounding sediments, making the sediment appear pervasively altered. This alteration is evident in thin sections that show patches of chloritic sediment, cloudy volcanic glass fragments, and corroded radiolarian tests.

Microstructurally, the fault gouge consists of angular and rounded lumps of slightly cemented silty clay, of all sizes from tens of µm to tens of millimeters diameter, and small pebbles of volcanic rock, in a cataclastic matrix (Pl. 4, Figs. 1, 2). Much of the matrix has a chaotically swirled fabric that gives the impression that the sediment has been subjected to a high degree of turbulent-mode shearing (in the sense of Lupini et al., 1981), while some patches appear to have escaped such intense deformation. Only the cemented siltstone blocks preserve any vestige of original bedding fabric. In BSE imaging, inclusions show all stages of cementation by silica and carbonate. In some inclusions, ferroan dolomite grows over and partly replaces detrital and authigenic quartz (Pl. 4, Fig. 4). A number of the siltstone clasts are cataclasites that have been recemented, and a few show incipient pressure-solution cleavage. It seems that while some of the inclusions were hard and rolled passively or were fractured to form angular fragments, others were soft pellets of clay that were squashed into ellipsoidal shapes or streaked out in the shearing.

Also present in all of the fault zone samples is gypsum, sometimes as stellate aggregates up to a millimeter across, but more commonly as fragmented and streaked-out patches (Pl. 4, Fig. 3). The concentration of deformed gypsum in a number of shear zones shows that it is a true authigenic mineral and certainly is not an artifact of sediment drying. In places, carbonate has preferentially cemented parts of the cataclastic matrix.

There was little core recovered from the main faulted interval in Hole 892A, but the microstructures in a sample from 117 mbsf show many features similar to those described above. Although the two holes are only 20 meters apart, there is no succession of structural features that can be matched unambiguously between them to define a single major fault plane.

Heterogeneous Deformation, 117–140 mbsf

In this depth range in both Holes 892A and 892D, some samples show intense fracturing or concentrations of small shear zones, while others are undeformed. There is no consistent style of deformation.

Deeper Fractured Interval, 140–165 mbsf

Samples from below about 140 mbsf show a greater intensity of deformation, but no large fault zones were encountered. Partitioning between brecciation in the diatomaceous silty portions and broad arrays of shear zones in the clayey portions (Pl. 5, Fig. 5), is again evident. In the more diatomaceous silty layers, shear zones are thin and crisscross the sediment nearly orthogonally, defining a mosaic structure identical to that described from shallower levels. In the clay-rich layers, the shear zones anastomose in subparallel arrays that cross at low angles, dividing the sediment into sigmoidal or rhombohedral domains. Some of the shear zones are lined with clays that either segregated into the zones of slip or formed in the fractures as secondary minerals. These clay-coated surfaces have become striated and polished, so at this deeper level the scaly fabric is better developed than in the shallower fractured interval.

Summary of Site 892 Deformation

The sediments from Site 892 are more intensely deformed than those examined from Sites 889 and 890, despite their similar positions in the interior parts of the wedge. This we attribute to the presence of fault zones at Site 892, each with a surrounding "damage zone" of subsidiary microstructures. The present-day hydrogeologically active fault is apparently dilatant, and is defined in the core by an interval of fractured and weakly scaly silts. In contrast the main gouge-filled fault zones we observed are highly compacted and so are unlikely to enable fluids to flow preferentially along them at the present day (Westbrook, Carson, Musgrave, et al., 1994).

The deformational styles at Site 892 are also markedly different from those at Site 891. There is practically no ductile deformation, such as folding, at Site 892, while distributed brittle fracturing is more common. We believe that the differences reflect contrasts in sediment properties that are partly due to greater compaction and lithification more landward in the wedge, and partly caused by the intrinsically more brittle nature of the diatomaceous silty clays predominant at Sites 889/890 and 892.

DISCUSSION: MECHANICAL IMPLICATIONS OF MICROSTRUCTURES

Effective Stress Changes and Formation of the Blocky "Mosaic" Structure

The most widespread texture in the cores from the accretionary wedge sites consists of discrete, very narrow fractures, with little or no shear offset, that divide the sediment into angular blocks. Material within the blocks is undeformed: sedimentary structures and delicate microfossils are preserved intact. Electron microscopic observations at high magnification (>500×) show that the shear zones are more compact as a result of phyllosilicate preferred orientation, accompanied by minor grain breakage and pore collapse. The mosaic blocks have a fairly uniform size and do not appear to have been brecciated or disaggregated, so that the appearance of the texture varies from a similar feature, "hydraulic breccia," encountered at the Nankai prism, where a variety of different-sized angular blocks appear to float in a muddier matrix (Byrne et al., 1993; Maltman et al., 1993).

The fracture sets run at various angles through the sediment and occasionally intersect at high angles to one another, subtending angles of 60–90°. If the fractures represent conjugate sets formed during pure shear, then high intersection angles indicate low angles of mobilized internal friction coupled with high cohesion (Ramsay and Huber, 1987; Wood, 1990). These silts are, however, unlikely to have high cohesive strength because of their low clay content. The intersection angles are also too variable to be intersections of Riedel R1 and R2 shear sets (Ramsay and Huber, 1987). There may have been several previous phases of deformation involving different orientations, or rotations of the principal stresses. As a more simple alternative, we can view the wide range of angles of intersection as possible evidence of near-isotropic tensile failure.

While we acknowledge that the relationships between intersection angle, stresses and components of frictional strength also depend on strain rates (e.g., Vermeer, 1990), and are influenced by earlier structures (Wan et al., 1990), we believe that the above characteristics suggest that the mosaic structure formed under low levels of differential stress, with tensile brittle failure being the dominant mechanism. The brittle behavior of the sediment, although being enhanced by the silty compositions, suggests that it was overconsolidated and deformed on a trajectory of decreasing mean effective stress (e.g., Atkinson and Bransby, 1978; Law, 1981; Jones and Addis, 1985).

The most likely way to reduce mean effective stress in buried sediments, while maintaining a low value of differential stress, is through elevation of pore fluid pressures in the wedge (e.g., Platt, 1990). Given the low inferred tensile strength of these silty sediments, the level of overpressure required to form the mosaic structure does not need to be large.

The inference of elevated pore fluid pressures does not necessarily require that exogenous fluids were injected into the sediments. These fine-grained and presumably low permeability sediments could have developed transient overpressures if they were subjected to rapid stress changes. Under these conditions, the sediment could fail in undrained shear (Yassir, 1990), and if they were already overconsolidated, as physical properties indicate (Westbrook, Carson, Musgrave, et al., 1994), then they could have undergone considerable dilation, possibly through tensile fracturing. A similar mechanism of hydraulic fracturing coupled with externally imposed stresses is suggested for other accretionary wedges by Behrmann (1991), and Brown (Brown et al., 1994a; K. Brown, pers. comm., 1994).

We appreciate that poroelastic or non-linear elastic mechanisms, not involving overpressuring, could also produce sets of near-orthogonal joints at depth (e.g., Engelder, 1993; Martel, 1994) but we believe they are unlikely to apply to the poorly lithified sediments at Cascadia (Brown et al., 1994b; Fischer and Engelder, 1994). It is probable that the fractures we observed formed through a combination of elevated pore pressures and stress release.

Transition into "Pillow-in-matrix" Structure and the Onset of Cataclasis

In places the blocky texture is modified by subsequent deformation, with the strain accommodated by the weakened material between the blocks. With further shearing, preferentially oriented fractures could develop into arrays of anastomosing shear zones. We see evidence of blocky texture being modified in this way in the vicinity of fault zones. The resulting structure consists of elongated lozenges or subrounded blocks (pillows) in a darker matrix. The matrix is formed of clays and silt-grade material, including fossil and mineral vein fragments, derived from the break-up of the blocks.

Widespread grain breakage is generally indicative of a high effective confining stress during deformation (Knipe, 1986; Lucas and Moore, 1986). However, while carbonate crystals, gypsum crystals, and siliceous fossils are commonly broken within the shear zones, we found few unequivocal occurrences of mechanically tough grains, such as quartz or feldspars, being broken in this way. Therefore, we do not believe that effective stresses, or burial depths were particularly great at the time of deformation. In some cases (e.g., Pl. 5), the mosaic blocks have undergone considerable rearrangement while suffering little internal damage. It is possible that in these cases deformation occurred at such low effective stresses that the blocks were kept apart by tensile failure and slid past one another passively. In other cases, the matrix grains apparently flowed past one another without cataclasis (independent particulate flow, sensu Borradaile, 1981), thus giving the "swirled" fabric evident in many samples with pillow structure.

Incipiently Scaly Fabric

Clay-rich silts in the vicinity of fault zones at Sites 891 and 892 commonly develop a fabric of anastomosing shear zones. This is similar to scaly fabric (sensu Moore et al., 1986a) in appearance, but is somewhat less pervasive and the surfaces are less lustrous than true scaly clay (Agar et al., 1989). The fact that the scaly fabric is not very well developed need not imply that the overall amount of strain was small, but rather implies that each slip surface accommodated little displacement, and so did not become well polished. If purer clays were present in the section, it is possible that these horizons, being weaker in simple shear, would have localized much of the deformation and generated true scaly clays.

Strain Hardening, Localization, and Partitioning of Pure and Simple Shear

Some of the contrasts between microstructures of diatomaceous silts and clayey silts/silty clays can be explained by their response to strain. In the diatomaceous silts, the shear zones probably strain-harden through coupled processes of grain breakage and collapse that lead to greater frictional interlocking of fragments and wall material. Further strain will tend to occur outside of the hardened shear zones, causing delocalization.

Shearing of clay-rich silts rapidly causes a preferred orientation of clay particles (Arch et al., 1988). In turn, this enables a laminar mode of shearing to develop, with reduced inter-particle friction leading to a lower residual strength (Lupini et al., 1981; Skempton, 1985). Thus, during bulk shear of bedded sediments, the clay-rich layers, being weaker, will sequester deformation progressively into localized zones. The shear zone geometries in the samples from Sites 891 and 892 provide some evidence for the operation of this mechanism. In the deformed clayey sediments, the shear zone sets characteristically display low angles of intersection. If these sets formed during pure shear (i.e., a finite strain of oblate flattening), they would suggest that high angles of internal friction were mobilized within the sediment and that it had low apparent cohesion (e.g., Wood, 1990). This inference is unreasonable: given the clayey nature of the sediment we would generally expect the reverse to apply. One possible explanation for the low intersection angles of the shear zones in these lithologies is that the sets formed in a conjugate Riedel arrangement during simple shear (i.e., a finite strain of prolate extension). We therefore speculate that the clay-rich horizons may accommodate deformation more readily during simple shear than during pure shear.

Compacted Gouge Zones and Inherited Deformation

It is notable that the deformational style and associations of authigenic minerals are very similar in fault zones from 20 and 113–116 mbsf in Hole 892D and at about 117 mbsf in Hole 892A. There appears to be a coherent succession of diagenesis and deformation in the mature fault zones at different levels of the site.

The clasts within the gouge zones show features that suggest a much greater degree of diagenesis, and higher strain than the immediate surroundings. The clasts appear, initially, to have been reworked from an earlier deformational episode. However, detailed electron optical observations reveal a progression from minor cementation by small amounts of carbonate outside the fault zones, to patchy but locally strong cementation within them. Parts of the gouge matrix are cemented by carbonate and gypsum, while some of the harder blocks are strongly lithified by multistage silica and carbonate cements and then re-deformed, to give overprinting relationships similar to those described from the Shimanto Belt of Japan (Agar, 1990). Similar cements are present in carbonate nodules scattered throughout the deformed and undeformed sections.

Implications for Fluid Flow in the Cascadia Accretionary Prism

We have suggested that the blocky mosaic texture prevalent in the landward sites is indicative of (at least transient) elevated pore fluid pressures in the interior of the Cascadia wedge. The presence of interconnected joint sets, whatever their origin, has important implications for fluid flow. While the blocks were held apart by high pore fluid pressures, fluid flow was presumably focused in the fracture network between them, thus establishing an efficient mechanism to dissipate the excess fluids.

Fractures held open over a wide area could promote diffuse dewatering, accompanied by rapid heat and chemical advection, though sequences that otherwise have low matrix permeability. Such enhanced flow could have caused the observed increase in chemical alteration and mineralization within the matrix of the pillow structure and in the gouge zones.

The interpretation that the fault zones were conduits for fluid flow requires that they were more permeable than the surrounding sediments. This does not agree with the present observation that the gouge zones are firmer and more compact than the wall sediments. This increased compaction would make the fault zone material less permeable than the surrounding undeformed sediment. If the gouge-filled fault zones were ever fluid conduits in the past, then they must have had a more open pore structure, which has subsequently collapsed and/or become occluded.

A possible mechanism for this flow-collapse sequence is continued shearing after a pulse of high pore fluid pressure caused an initial period of dilation (Knipe, 1986; Moore and Byrne, 1987). In this case, the sediment would experience a combination of renewed compaction due to the increase in effective stress, and fabric collapse due to shear-induced particle preferred orientation (Arch and Maltman, 1990). The localization of the deformation into clay-rich shear zones suggests that this latter process was indeed important, with the sediment going beyond the critical state and approaching conditions of residual shearing along a small number of weaker slip planes (see Atkinson and Bransby, 1978; Skempton, 1985). Significant dilation is then required to enable such compacted fault gouge material to conduct fluids during a subsequent cycle. Recent experiments in a ring shear device capable of imposing residual shearing conditions on clays at high stresses (Brown et al., 1994a) demonstrate the feasibility of this general mechanism and suggest that localized hydraulic fracturing may be important in re-opening the flow conduits within muddy fault zones.

SUMMARY

The principal scientific objective of Leg 146 was to investigate the relative roles of diffuse and fault-focused fluid flow in accretionary wedges. We believe that the microstructures we have described provide evidence of both high pore-fluid pressures and fluid flow through fault and fracture systems in the landward part of the Cascadia accretionary wedge. Despite the problems of representative sampling, the microstructural results are compatible with the geophysical and shipboard data defining the larger scale structure of the prism. We are not able to reconstruct in detail tectonic events at Site 891 from the limited material recovered intact from cores, but we can define the main structural styles. In contrast, the density of microstructural observations from Site 892 enables us to offer considerable refinement of the structural and hydrogeological evolution of this part of the prism.

Overpressuring, caused by rapid burial or tectonic loading, may have been responsible for the widespread occurrence of tensile fracturing and mosaic structure in the wedge sediments. Alternatively, we suggest that undrained shear could have played a role in developing localized dilatant fracturing in overconsolidated sediments of the wedge. We believe that deformation under drained conditions led to residual-state shearing and enhanced compaction in mature fault zones. This faulting produced either "turbulent" structures such as pillow structure and gouge in silts, or "laminar" fabrics such as incipient scaly structure and shear-zone arrays in clay-rich sediments (see Lupini et al., 1981). Alternation between rapid, undrained failure and slower, drained deformation may have produced some of the complex overprinting relationships we observe in the fault zones.

ACKNOWLEDGMENTS

Ben Clennell acknowledges the support of the Natural Environment Research Council (United Kingdom) in funding this work, first as part of an ODP Special Topic, and second through an extraordinary payment for additional microstructural studies. Graham Westbrook, University of Birmingham, Kevin Brown of Scripps Institution of Oceanography, San Diego, and Rob Knipe at the University of Leeds provided ideas and support. Help with electron microscopy was provided by Geoff Lloyd. Many of the principal interpretations of the macroscopic structures originate from the excellent shipboard work of Harold Tobin.

The reviewers and editors are thanked for their careful work, which has improved the clarity and scientific content of this paper.

REFERENCES

Agar, S.M., 1990. The interaction of fluid processes and progressive deformation during shallow level accretion: examples from the Shimanto Belt of SW Japan. *J. Geophys. Res.*, 95:9133–9148.

Agar, S.M., Prior, D.J., and Behrmann, J.H., 1989. Back-scattered electron imagery of the tectonic fabrics of some fine-grained sediments: implications for fabric nomenclature and deformation processes. *Geology*, 17:901–904.

Arch, J., and Maltman, A., 1990. Anisotropic permeability and tortuosity in deformed wet sediments. *J. Geophys. Res.*, 95:9035–9045.

Arch, J., Maltman, A.J., and Knipe, R.J., 1988. Shear-zone geometries in experimentally deformed clays: the influence of water content, strain rate and primary fabric. *J. Struct. Geol.*, 10:91–99.

Atkinson, J.H., and Bransby, P.L., 1978. *The Mechanics of Soils: An Introduction to Critical State Soil Mechanics:* London (McGraw-Hill).

Behrmann, J.H., 1991. Conditions for hydrofracture and fluid permeability of accretionary edges. *Earth Planet. Sci. Lett.*, 107:550–558.

Borradaile, G.J., 1981. Particulate flow and the formation of cleavage. *Tectonophysics*, 72:305–321.

Brown, K.M., Bekins, B., Clennell, B., Dewhurst, D., and Westbrook, G.K., 1994a. Heterogeneous hydrofracture development and accretionary fault dynamics. *Geology*, 22:259–262.

————, 1994b. Heterogeneous hydrofracture development and accretionary fault dynamics: reply. *Geology*, 22:1053–1054.

Byrne, T., Maltman, A., Stephenson, E., Soh, W., and Knipe, R., 1993. Deformation structures and fluid flow in the toe region of the Nankai accretionary prism. *In* Hill, I.A., Taira, A., Firth, J.V., et al., *Proc. ODP, Sci. Results*, 131: College Station, TX (Ocean Drilling Program), 83–101.

Cochrane, G.R., MacKay, M.E., Moore, G.F., and Moore, J.C., 1994. Consolidation and deformation of sediments at the toe of the central Oregon accretionary prism from multichannel seismic data. *In* Westbrook, G.K., Carson, B., Musgrave, R.J., et al., *Proc. ODP, Init. Repts.*, 146 (Pt. 1): College Station, TX (Ocean Drilling Program), 421–426.

Cowan, D.S., 1985. Structural styles in Mesozoic and Cenozoic melanges in the western Cordillera of North America. *Geol. Soc. Am. Bull.*, 96:451–462.

Engelder, T.J., 1993. *Stress in the Lithosphere:* New York (Princeton).

Farrell, S.G., and Eaton, S., 1988. Foliations developed during slump deformation of Miocene marine sediments, Cyprus. *J. Struct. Geol.*, 10:567–576.

Fischer, M.P., and Engelder, T.J., 1994. Heterogeneous hydrofracture development and accretionary fault dynamics: comment. *Geology*, 22:1052–1053.

Hyndman, R.D., Spence, G.D., Yuan, T., and Davis, E.E., 1994. Regional geophysics and structural framework of the Vancouver Island margin accretionary prism. *In* Westbrook, G.K., Carson, B., Musgrave, R.J., et al., *Proc. ODP, Init. Repts.*, 146 (Pt. 1): College Station, TX (Ocean Drilling Program), 399–419.

Jones, M.E., and Addis, M.A., 1985. The application of stress-path and critical state analysis to sediment deformation. *J. Struct. Geol.*, 8:575–580.

Karig, D.E., 1990. Experimental and observational constraints on the mechanical behavior in the toes of accretionary prisms. *In* Knipe, R.J., and Rutter, E.H. (Eds.), *Deformation Mechanisms, Rheology and Tectonics.* Geol. Soc. Spec. Publ. London, 54:383–398.

Knipe, R.J., 1986. Faulting mechanisms in slope sediments: examples from Deep Sea Drilling Project cores. *In* Moore, J.C. (Ed.), *Structural Fabric in Deep Sea Drilling Project Cores from Forearcs.* Mem.—Geol. Soc. Am., 166:45–54.

Law, K.T., 1981. Effect of stress path geometry on soil brittleness. *Geotechnique*, 31:279–287.

Lucas, S.E., and Moore, J.C., 1986. Cataclastic deformation in accretionary wedges: Deep Sea Drilling Project Leg 66, southern Mexico, and on-land examples from Barbados and Kodiak Island. *In* Moore, J.C. (Ed.), *Structural Fabric in Deep Sea Drilling Project Cores from Forearcs.* Mem.—Geol. Soc. Am., 166:89–103.

Lupini, J.F., Skinner, A.E., and Vaughan, P.R., 1981. The drained residual strength of cohesive soils. *Geotechnique*, 31:181–213.

MacKay, M.E., Moore, G.F., Cochrane, G.R., Moore, J.C., and Kulm, L.D., 1992. Landward vergence and oblique structural trends in the Oregon margin accretionary prism: implications and effect on fluid flow. *Earth Planet. Sci. Lett.*, 109:477–491.

Maltman, A., 1994. Prelithification deformation. *In* Hancock, P.L. (Ed.), *Continental Deformation:* Oxford (Pergamon).

Maltman, A.J., Byrne, T., Karig, D.E., and Lallement, S., 1993. Deformation at the toe of an active accretionary prism: synopsis of results from ODP Leg 131, Nankai, SW Japan. *J. Struct. Geol.*, 15:949–964.

Martel, S.J., 1994. On the paradox of systematic, contemporaneous, orthogonal opening-mode fractures. *In* Nelson, J., and Laubach, P. (Eds.), *Rock Mechanics.* Proc. 1st North Am. Rock Mech. Symp., 801–808.

Moore, J.C., 1989. Tectonics and hydrogeology of accretionary prisms: role of the décollement zone. *J. Struct. Geol.*, 11:95–106.

Moore, J.C., and Byrne, T., 1987. Thickening of fault zones: a mechanism of melange formation in accreting sediments. *Geology*, 15:1040–1043.

Moore, J.C., Mascle, A., et al., 1990. *Proc. ODP, Sci. Results*, 110: College Station, TX (Ocean Drilling Program).

Moore, J.C., Roeske, S.M., Lundberg, N., Schoonmaker, J., Cowan, D.S., Gonzales, E., and Lucas, S.E., 1986. Scaly fabrics from Deep Sea Drilling Project cores from forearcs. *In* Moore, J.C. (Ed.), *Structural Fabric in Deep Sea Drilling Project Cores From Forearcs.* Mem.—Geol. Soc. Am., 166:55–73.

Moore, J.C., and Vrolijk, P., 1992. Fluids in accretionary prisms. *Rev. Geophys.*, 30:113–135.

Platt, J.P., 1990. Thrust mechanics in highly pressured accretionary wedges. *J. Geophys. Res.*, 95:9025–9034.

Ramsay, J.R., and Huber, M.I., 1987. *The Techniques of Modern Structural Geology* (Vol. 2): *Folds and Fractures:* London (Academic).

Shipboard Scientific Party, 1994. Leg 146 introduction: Cascadia Margin. *In* Westbrook, G.K., Carson, B., Musgrave, R.J., et al., *Proc. ODP, Init. Repts.*, 146 (Pt. 1): College Station, TX (Ocean Drilling Program), 5–14.

Skempton, J.A.W., 1985. Residual strength of clays in landslides, folded strata and the laboratory. *Geotechnique*, 35:3–18.

Vermeer, P.A., 1990. The orientation of shear bands in biaxial tests. *Geotechnique*, 40:223–236.

Wan, A.W.L., Graham, J., and Gray, M.N., 1990. Influence of soil structure on the stress-strain behaviour of sand-bentonite mixtures. *Geotech. Test. J.*, 13:179–187.

Westbrook, G.K., 1991. Geophysical evidence for the role of fluids in accretionary wedge tectonics. *Philos. Trans. R. Soc. London A*, 335:227–242.

————, 1994. Growth of accretionary wedges off Vancouver Island and Oregon. *In* Westbrook, G.K., Carson, B., Musgrave, R.J., et al., *Proc. ODP, Init. Repts.*, 146 (Pt. 1): College Station, TX (Ocean Drilling Program), 381–388.

Westbrook, G.K., Carson, B., Musgrave, R.J., et al., 1994. *Proc. ODP, Init. Repts.*, 146 (Pt. 1): College Station, TX (Ocean Drilling Program).

Wood, D.M., 1990. *Soil Behaviour and Critical State Soil Mechanics:* Cambridge (Cambridge Univ. Press).

Yassir, N., 1990. The undrained shear behavior of fine sediments. *In* Knipe, R.J., and Rutter, E.H. (Eds.), *Deformation Mechanisms, Rheology and Tectonics.* Geol. Soc. Spec. Publ. London, 54:399–404.

Date of initial receipt: 6 September 1994
Date of acceptance: 31 March 1995
Ms 146SR-215

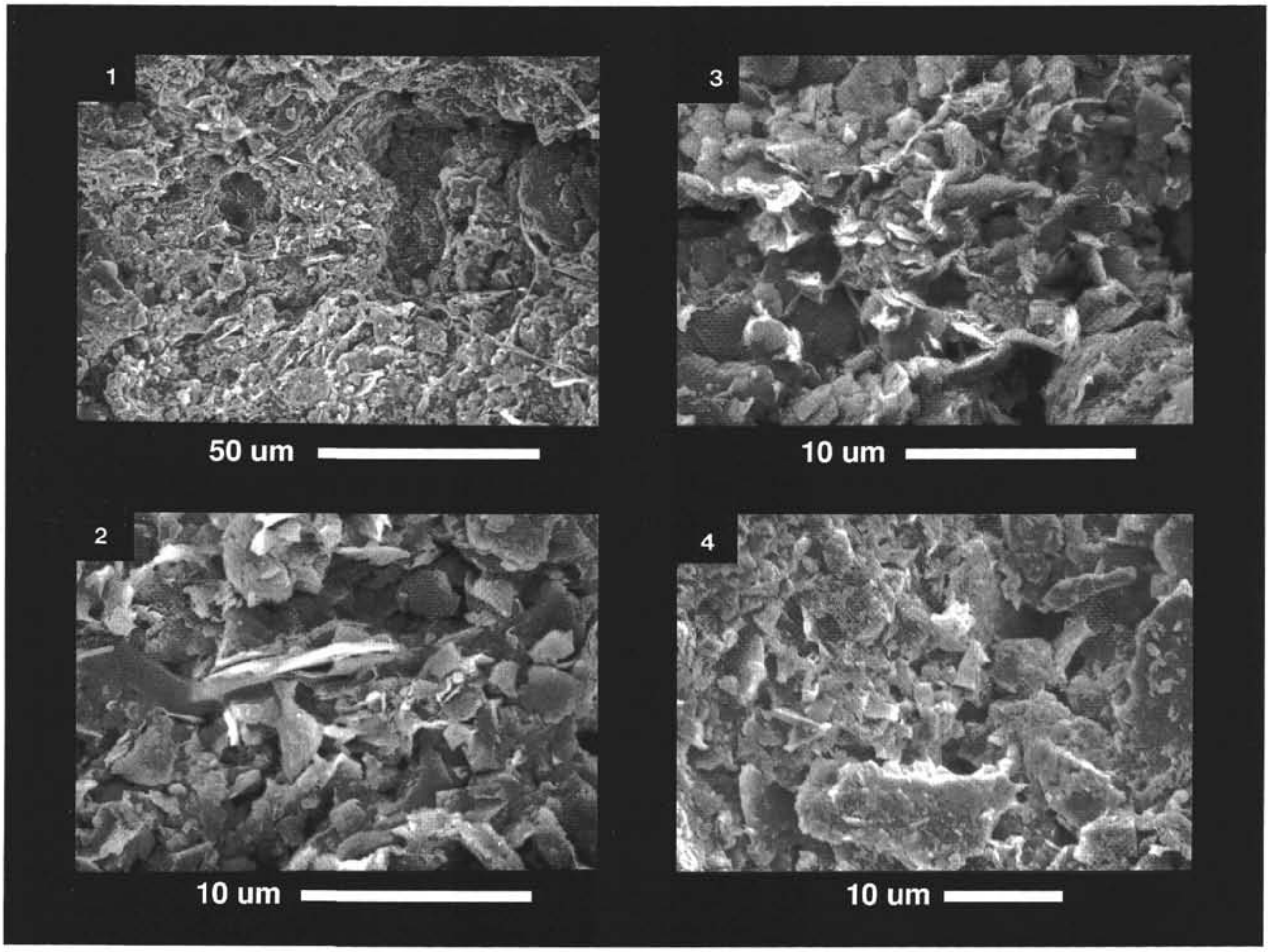

Plate 1. Secondary electron images of microfabrics in undeformed sediments from Leg 146 cores. **1.** Sample 146-892A-1X-1, 34–36 cm (0.3 mbsf). Clayey silt with aggregated structure showing large inter-aggregate pores, and lack of any preferred grain alignment. **2.** Close-up of same sample showing open fabric and high intra-aggregate porosity. Large grain in center is a fresh volcanic glass fragment. **3.** Sample 146-892E-1X-2, 20–22 cm (0.5 mbsf), a highly porous silty clay. Note lack of preferred grain alignment and pores bridged by chains of clay particles in face-to-edge contact. **4.** Sample 146-891B-40X-1, 134–137 cm (305.34 mbsf). Sandy silt with incipient carbonate cement.

This page intentionally left blank.

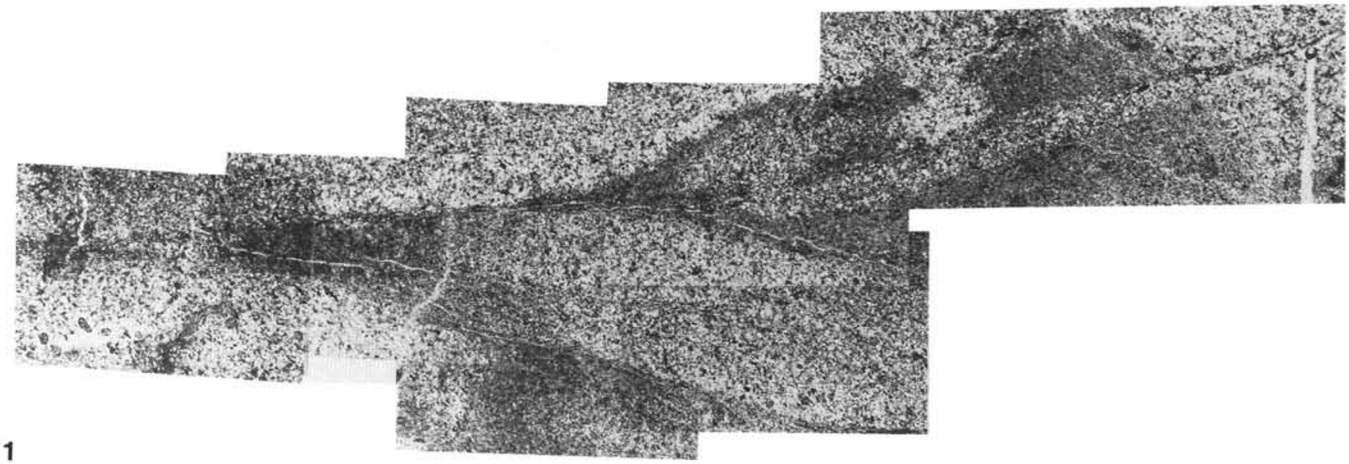

1

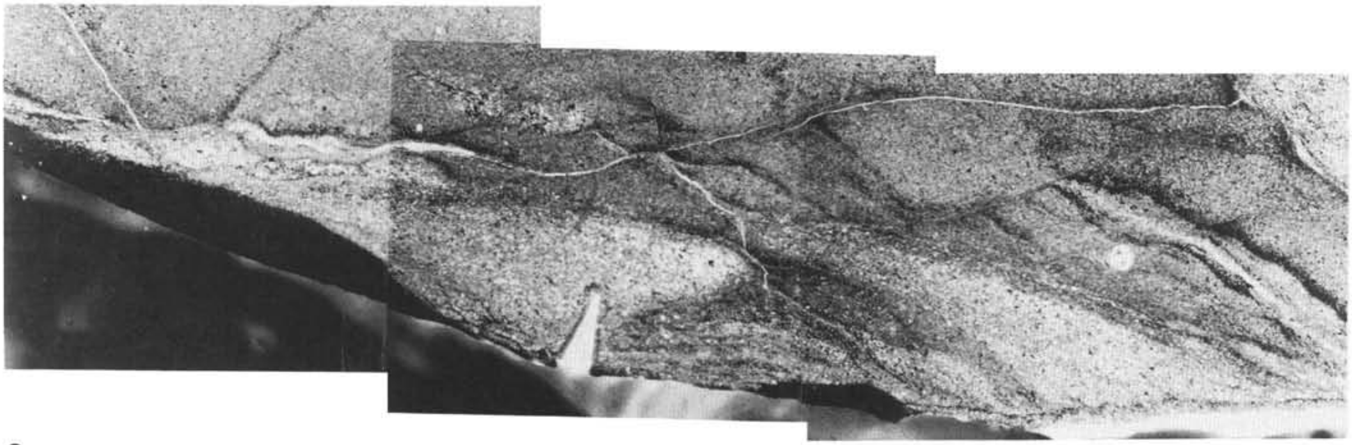

3

Plate 2. Soft-sediment deformation structures from Site 891. **1, 2.** Sample 146-891B-31X-CC, 20–22 cm (244 mbsf). Interlayered sand and clayey silt showing small sediment-loading structures overprinted by discrete shear zones that cut through the sediment without causing any grain breakage. **3, 4.** Sample 146-891B-45X-1, 43–45 cm (349 mbsf). Ripple cross-laminated silty clay and silt, with small sediment-loading structures, later affected by stratal extension that produces microfaults and ductile kink zones, with no grain breakage or enhanced particle alignment.

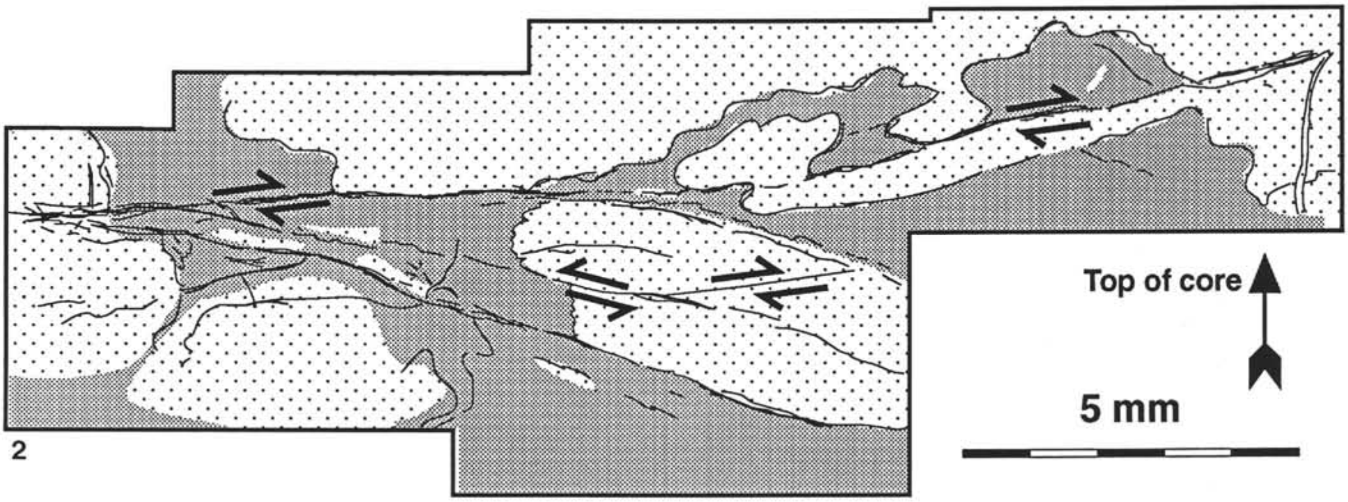

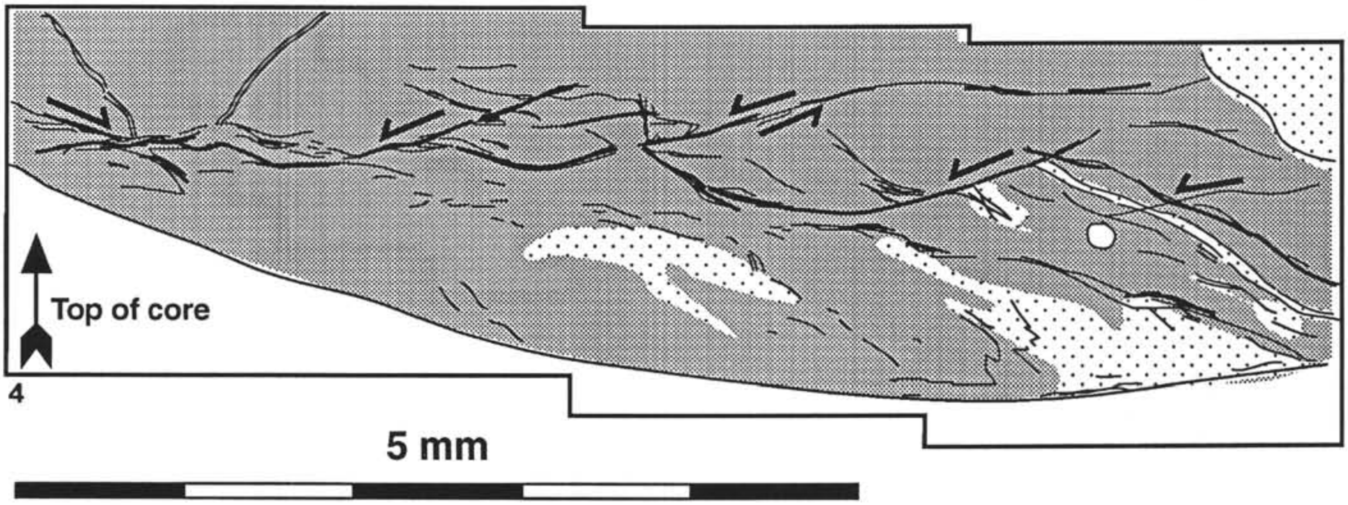

Plate 2 (continued).

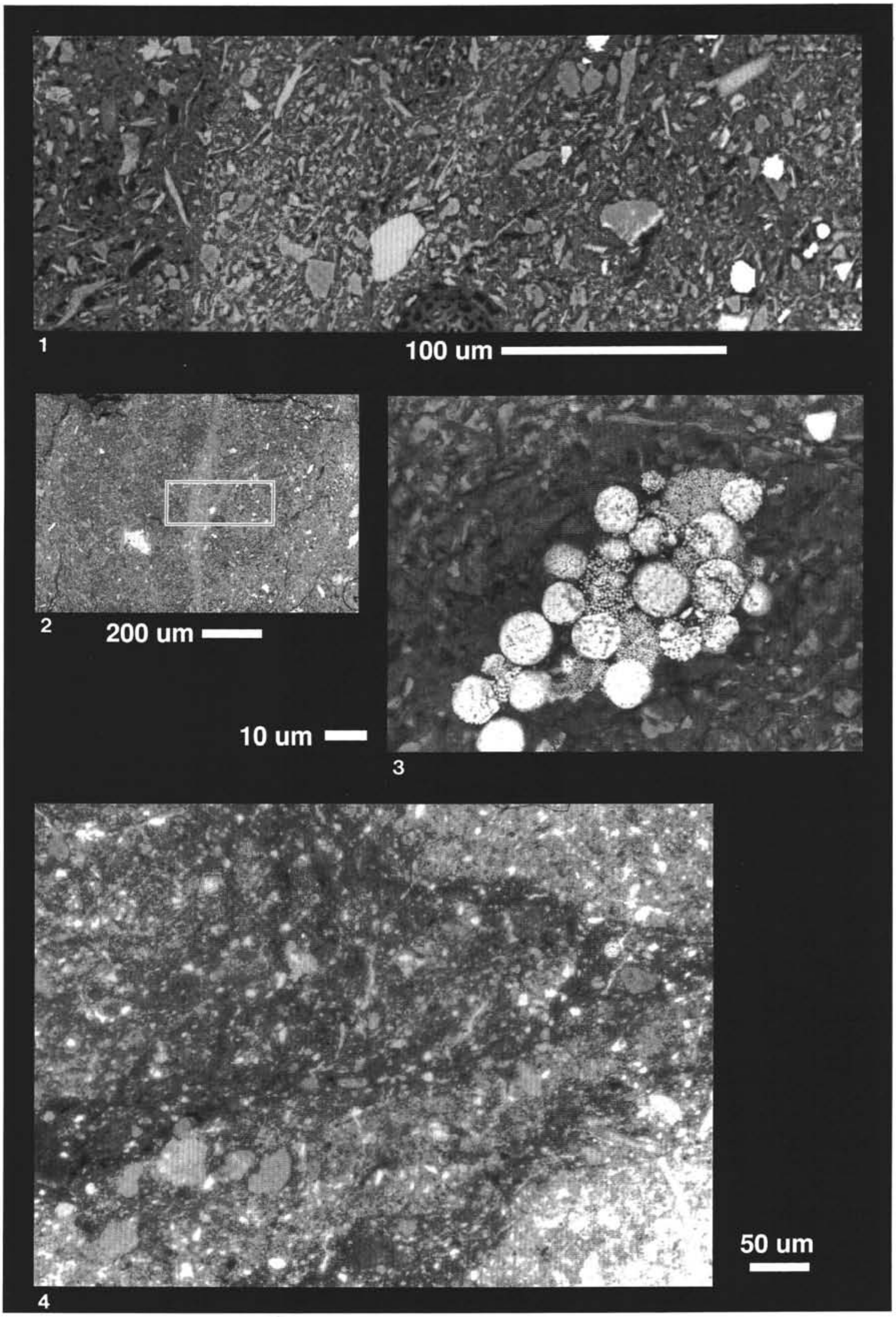

Plate 3. **1.** Close-up of box in (2). **2.** Backscattered electron images of Sample 146-892D-10X-3, 111–116 cm (103 mbsf). Broad shear zones with diffuse edges developed in clayey silt with high proportion of siliceous microfossils. Shear zones appear brighter because of enhanced compaction accompanying cataclasis and particle alignment. **3.** Pyrite, as microframboidal aggregates, is almost ubiquitous in fine-grained sediments from the Cascadia Margin. Backscattered electron image of Sample 146-891B-40X-2, 53–54 cm (306 mbsf). **4.** Glaucony sand showing broad, darker shear zones that separate diffuse-edged patches of paler, undeformed sediment. Some glaucony grains appear to overgrow the grain alignment fabric in the clay-rich shear zones. Plane-polarized light.

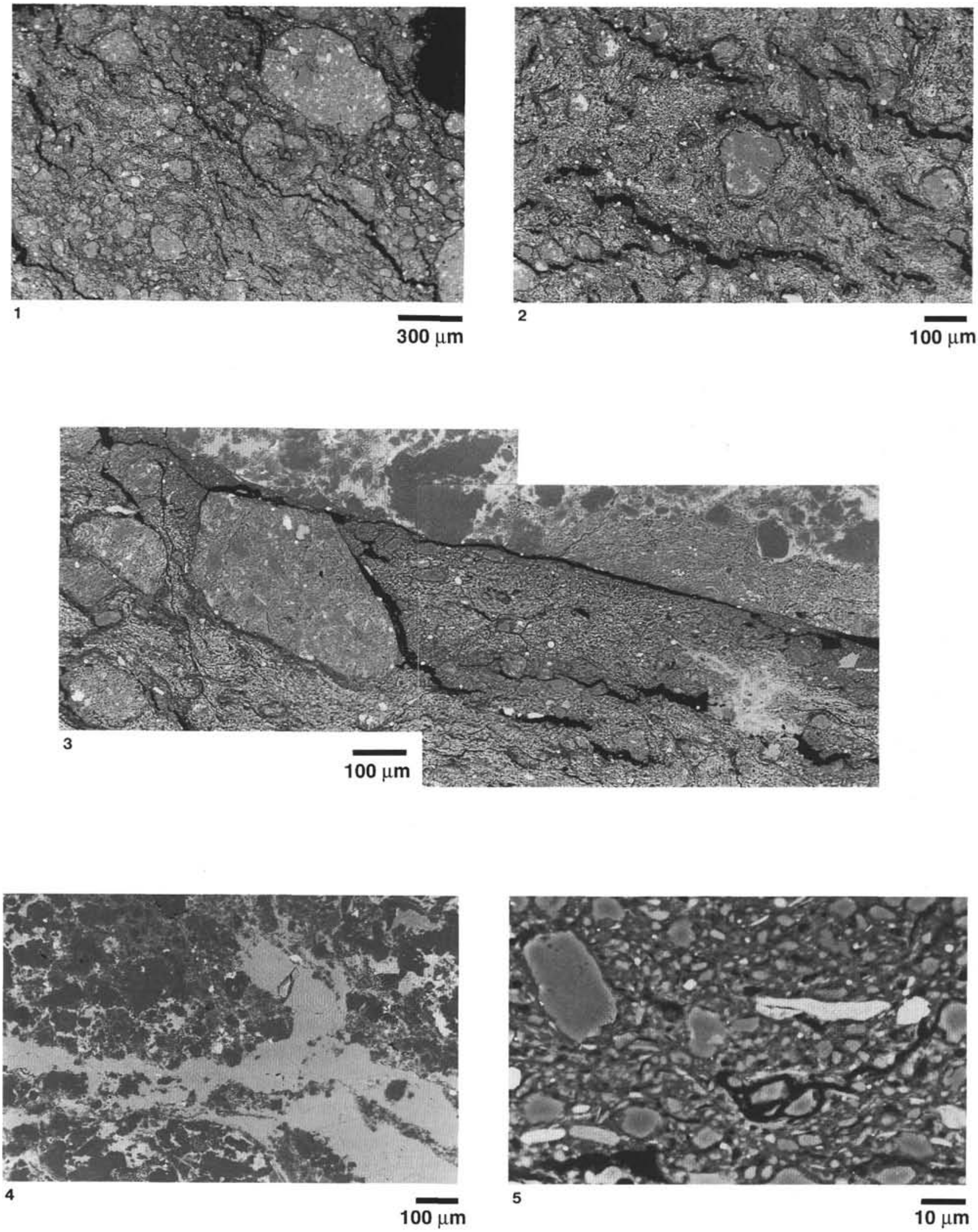

Plate 4. Backscattered electron images of fault gouge zones at Site 892. **1.** Typical microstructure of hard and soft clasts within comminuted and foliated matrix developed in fault gouge; Sample 146-892D-2X-2, 16–22 cm (10 mbsf). **2.** Nearly identical microstructures in Sample 146-892D-10X-6, 69–74 cm (107 mbsf), from the main fault zone at this site. **3.** Large, highly cemented clast, to top of picture, with an envelope of sheared, cataclastic material. The spidery white patch in the matrix to the far left is a deformed aggregate of gypsum crystals. Sample 146-892D-10X-4, 45–50 cm (104 mbsf), from near the top of the main fault zone. **4.** Calcite veins (middle gray) in a clast within the gouge that is strongly cemented by quartz (dark gray) and ferroan dolomite (white). **5.** Close-up of cataclastic material enveloping large block, located at extreme right of (3) at arrow.

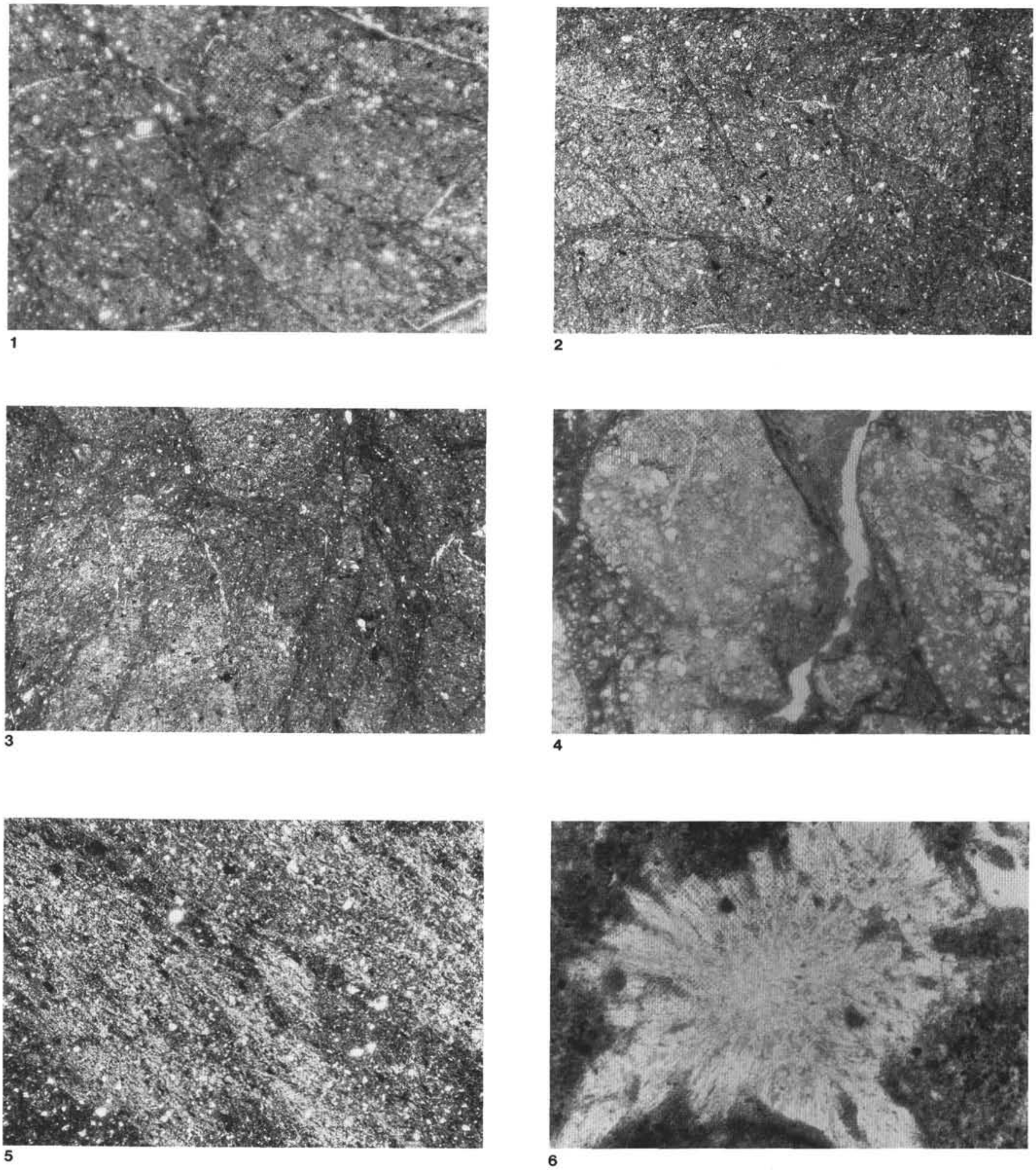

Plate 5. **1.** Mosaic texture defined by discrete fractures that divide the diatomaceous, clayey silt into blocks. Sample 146-892D-16X-5, 104–107 cm (164 mbsf). **2.** Blocky mosaic structure in clayey silt from 30 centimeters below (1). **3.** Transition into pillow-in-matrix structure in same sample. Note broader, dark shear zones, that are rich in clays, and diffuse block edges. **4.** Gouge zone, Sample 146-892D-10X-4, 45–50 cm (104 mbsf). Appearance is distinct from pillow-in-matrix structure, as internally the inclusions are cemented and/or show cataclasis. **5.** Aligned phyllosilicate particles define a broad shear zone in clayey silt. Sample 146-892A-18X-1, 63–64 cm (145 mbsf). **6.** Stellate aggregate of gypsum crystals from within main fault zone, 107 mbsf, Hole 892D. Photographs 1, 2, 3, 4, 6 = plane polarized light; photograph 5 = crossed polars. Photo widths: 1, 4, 6 = 1.5 mm; 2, 3, 5 = 4.5 mm.